Pore formation during reactive sintering of iron-aluminium powder mixtures

M. Knüwer
Fraunhofer-Institute for Manufacturing and Advanced Materials, Bremen, Germany

Abstract

During reactive sintering of iron and aluminium a significant swelling effect with the generation of porosity can be detected, depending on the parameters of the sintering process. This undesired effect can possibly be used for the generation of a functional porosity e.g. in filter structures. Reactive sintering experiments of elemental powder mixtures were performed with different aluminium contents corresponding to the intermetallic phases $FeAl_2$, Fe_2Al_5 and $FeAl_3$. Depending on the aluminium content a linear swelling effect of max. 25% was reached. The resulting structures show a permeable porosity for gases and fluides and reach a density down to 1,8 g/cm³, equivalent to a porosity of about 50%. Further experiments characterise the microstructure, permeability and equivalent pore diameter of the structures. The experimental results show that reactive sintered iron aluminides could be a possible substitute for brass and stainless steel filters.

1. Introduction

Iron- and titanium aluminide intermetallic phases are interesting materials for structural or functional applications at elevated temperatures and in aggressive atmospheres [1, 2]. Compared to conventional iron based high temperature alloys their mechanical stability and oxidation resistance are significantly higher. A problem occurring with the application of aluminides is their difficult processing during production and shaping caused by the high brittleness of these materials. The brittleness of the aluminides is attributed to their complicated lattice structure and the higher amount of hetero- and homeopolar bonds between the atoms compared to conventional alloys [3]. Different ways to produce near net shape parts of aluminides were investigated, e.g. the Ceracon process [1] or Metal-Injection-Moulding (MIM) [4] combined with reactive-sintering of elemental powder mixtures. During reactive sintering an additional driving force for building a compact is given by the free energy of formation as shown in Fig. 1 for different aluminides [5].

It is easy to see that the free energy of formation of iron-aluminide is in general much lower as in the case of cobalt- or nickel-aluminides. The energy of formation determines the stability of the intermetallic phase. A high free energy is yields to a high phase stability. In the case of iron-aluminide the highest stability of the intermetallic phase occurs at 75 at.% aluminium, corresponding to the phase $FeAl_3$. In the iron-aluminium system two superlattice structures (Fe_3Al and FeAl) and three intermetallic phases ($FeAl_2$, Fe_2Al_5 and $FeAl_3$) occur as shown additionally in Fig. 1. A problem arising with the reactive sintering process of dense products is the swelling effect combined with an uncontrolled formation of porosity up to 50%. Many published papers are dealing with the decrease of porosity during reactive sintering by a variation of process parameters or the powder particle size [4, 6-9]. The discussed aluminides are Fe_3Al, Ti_3Al, TiAl and Ni_3Al. A good prediction of swelling behaviour is given *Böhm et*

J. Banhart, M.F. Ashby, N.A. Fleck: *Metal Foams and Porous Metal Structures.* © MIT Verlag (1999)

al. [10], but only up to an aluminium-content of 45 at.%; corresponding to the Phase TiAl. On the other hand it should be possible to maximise the swelling effect and the generation of pores in the compact to create a highly porous material with open porosity for applications as e.g. high temperature filter or catalytic converter carrier.

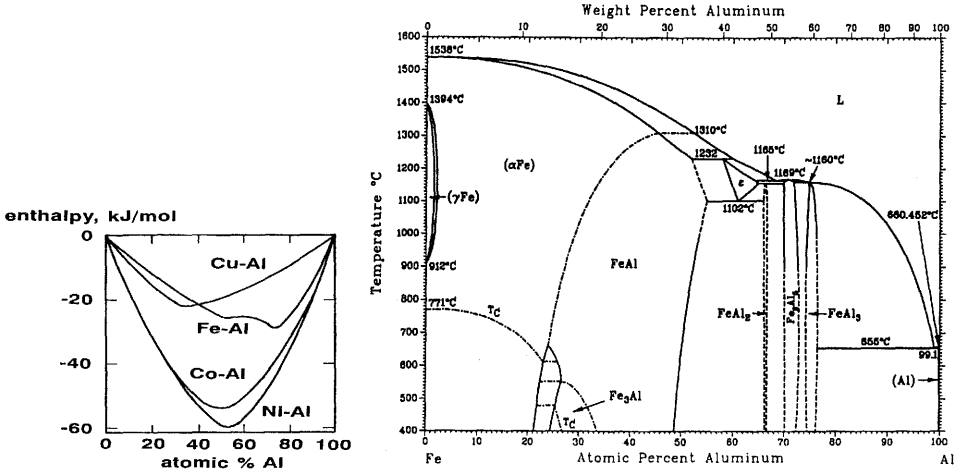

Fig. 1: Free energy of formation of aluminides and Fe-Al binary phase diagram

2. Experimental

The stoichiometry was chosen as variable parameter in work producing iron aluminides. The particle sizes of iron and aluminium powders were defined by sieving. The powders were mixed using a tumbling mixer and subsequently hot pressed for 50 minutes at a temperature of 500°C, resulting in a density around 97% of the theoretical density of powder mixture. After machining the samples were heated up to 750°C under normal atmosphere. The following powder-combinations were used:

Stoichiometry:		Particle size:	
$FeAl_2$: 50,9 w.% Fe	49,1 w.% Al	Fe < 63µm	Al 63-90µm
Fe_2Al_5:	45,3 w.% Fe 54,1 w.% Al	mean value 49,9 µm	mean value 74,8 µm
$FeAl_3$: 40,8 w.% Fe	59,2 w.% Al		

2.1 Pre-reaction effects

Fig. 2 shows a typical microstructure of a hot pressed elemental powder compact with a composition corresponding to $FeAl_3$. Three different phases are visible. The phases were investigated by EDX-analysis and represent the aluminium-matrix (1), pure iron (2) and the phase $FeAl_3$ (3). It is obvious that a reaction between iron and aluminium has taken place already during the hot pressing process, as the iron particles are covered by an approximately 15 µm thick layer of $FeAl_3$. Similar observations were made by *Böhm et al.* [10] during investigations on the Ti-Al-System. A model was proposed by *Savitskii* [11] for the growth of an intermetallic $TiAl_3$-layer on the iron particle surface, the instantaneous particle radius and the resulting macroscopic growth of the sample. It was confirmed and extended to a four stage model by *Böhm et al.* [10]. It was noticed that macroscopic swelling took place at a sample temperature above the melting temperature of aluminium.

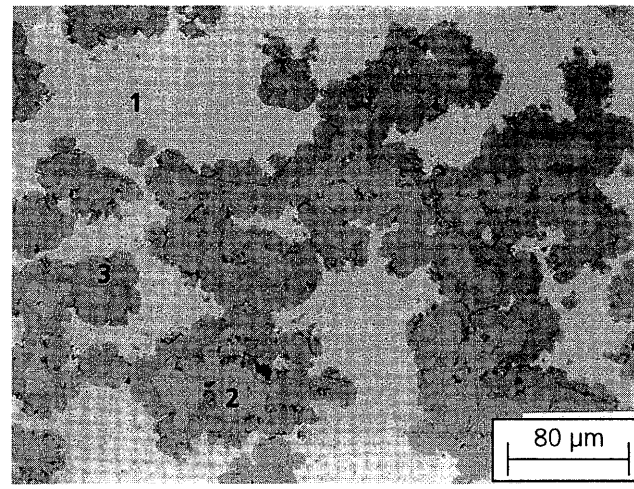

Fig. 2: Microstructure of an elemental powder compact corresponding to $FeAl_3$

2.2 Effects during reactive sintering

The reactive sintering of the specimen took place under normal atmosphere at a temperature of 750°C. The samples were placed in the hot furnace and heated up. The measured heating rate in the sample was around 80K/min. After visible melting of the aluminium the sample started to react immediately. The sample temperature went up to around 855°C. Fig. 3 characterises the expansion process during reactive sintering for a pressed sample with a composition corresponding to the phase $FeAl_3$. It can be seen that the expansion process starts after a time of 300 s, when sample temperature has reached 615°C. The Temperature difference between 615°C and the theoretical melting temperature of Fe-Al-eutectic can probably be attributed to the relatively high heating rate. Especially during the self propagating reaction with its extremely high heating rate a too low temperature is measured. Measurements with a second, faster working thermocouple delivered a higher maximum reaction temperature of 1097°C. So the sample temperature given in Fig. 3 should be interpreted with care.

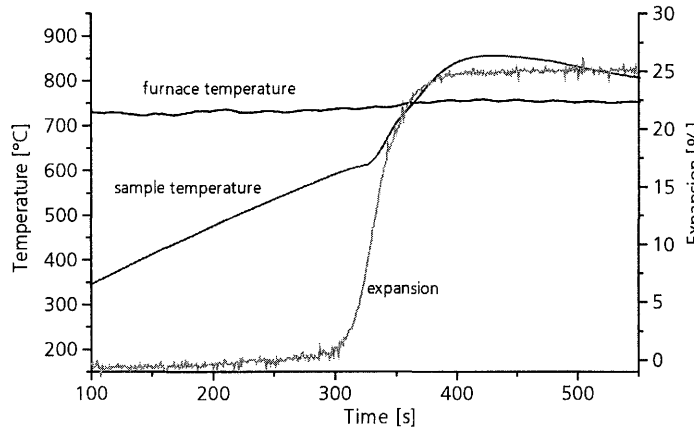

Fig. 3: Expansion during reactive sintering of $FeAl_3$

The heating during the self propagating reaction process starts approx. 20 s after the expansion has begun. At the beginning of the expansion, the released energy of formation is probably consumed by the heat of fusion of the aluminium. During this period the velocity of the reaction is still relatively low. In the following the reaction increases its velocity strongly, recognisable at the very high expansion rate. Nearly the whole expansion process is finished in about 40 s. Heating of the sample by energy of formation is continued after the end of the expansion and reaches its maximum after about 100 s.

2.3 Microstructure and permeability

According to *Savitskii* [11], the porosity after reactive sintering can be the influenced by powder particle size and stochiometry of the phase. The experiments described here are focused on the influence of phase stochiometry on porosity and permeability. A typical microstructure of reactive sintered $FeAl_2$ is shown in Fig. 4.

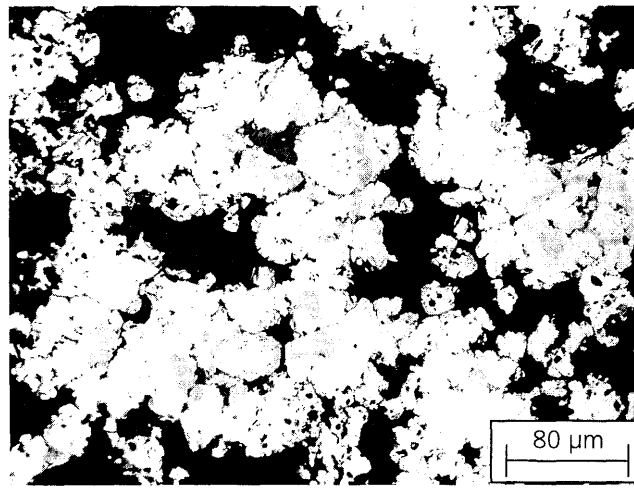

Fig. 4: Microstructure of reactive sintered $FeAl_2$ (black = pores)

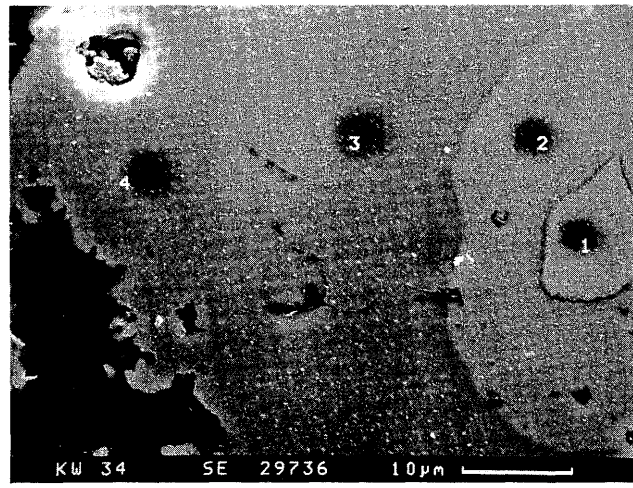

Fig. 5: SEM-micrograph with EDX-spots in a reaction sintered Fe-2Al-powder mixture

Fig. 4 shows different spot-like shaped phases in the reacted structure. EDX-analyses of this phases are shown in Fig. 5 in a higher magnified REM-micrograph. In the centre of such a spot (1) pure iron was detected. The next outer phase (2) shows a composition of 40.5 at.% Al and 59.5 at.% Fe, which corresponds to the two-phase region between the superlattice structure FeAl and the intermetallic phase $FeAl_2$, as shown in the binary phase diagram (Fig. 1). According to Fig. 1 at this point a two phase microstructure should be visible, but can not be detected on the micrograph. The third phase investigated at point (3) and (4) consists of 68.5 at.% Al and 31.5 at.% Fe, corresponding nearly to the intermetallic phase $FeAl_2$, but with a small excess on Aluminium.

In Fig. 6 it can be seen that in general the porosity, given by:

$$P = \frac{\rho_{sample}}{\rho_{theor.}} \cdot 100, \tag{1}$$

where P = porosity [%], ρ_{sample} = sample density; $\rho_{theor.}$ = theoretical density of the intermetallic phase and the equivalent pore diameter, given by

$$D_{eq} = \sqrt{\frac{32 \cdot L \cdot \dot{V} \cdot \eta}{A \cdot \Delta p \cdot P}}, \tag{2}$$

where D_{eq} is the equivalent pore diameter; L = sample length; $\dot{V}$ = flow rate; η = dynamic viscosity of the fluid; A = sample area; Δp = pressure loss; P = porosity

increase with increasing aluminium content. The pore diameter shows a stronger dependence on the aluminium content than the porosity. Although the porosity of the samples grows with increasing aluminium content only from 35 to 52 %, the equivalent pore diameter increases from 9.3 µm up to 24.3 µm. For the calculation of the equivalent pore diameter a permeability-test according to ISO 4022 was performed.

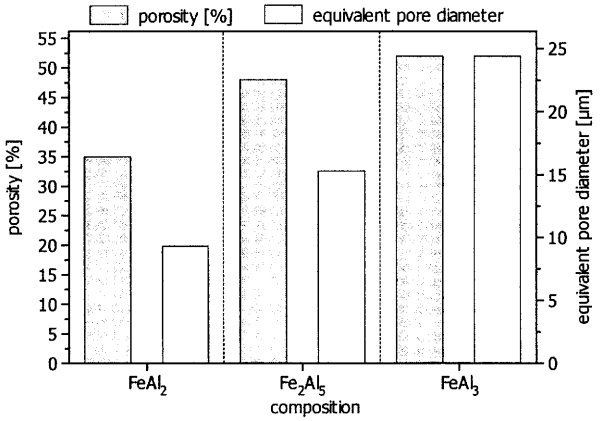

Fig. 6: Porosity and equivalent pore diameter of reactive sintered iron-aluminides

Additionally, with the ISO 4022 permeability test the determination of the filter coefficients α and β is possible. α describes the laminar flow, β the turbulent flow of a gas or fluid through the filter. α and β could be determined graphically by plotting formula (3).

$$\frac{\Delta p \cdot A}{\dot{V} \cdot L \cdot \eta} = \frac{1}{\beta} \cdot \frac{\dot{V} \cdot \rho}{A \cdot \eta} + \frac{1}{\alpha} \tag{3}$$

where Δp = pressure loss, A = sample area, $\dot{V}$ = flow rate, L = sample length, η = dynamic viscosity of the fluid, ρ= density of the fluid

With the permeability coefficients α and β it is possible to identify an appropriate filter for a given application.

3 Discussion

3.1 Pre-reaction effects

The publications mentioned above [8-11] do not describe the formation of a significant layer of an intermetallic phase consisting of Ti-, Ni- or $NbAl_X$ on the elemental metal powder during compaction. *Böhm et al.* [10] notice the growth of a thin intermetallic layer during the first stage of reaction sintering below the melting temperature of aluminium. In the work of *Dahms et al.* [8] and *Ferreira et al.* [9] the compaction of the specimen was performed at room temperature, so that the diffusion controlled growth of the layer cannot take place. A thermally treatment at 600°C leads to a very thin porous $TiAl_3$-layer on the titanium particles [8]. An ageing process for 24h at 550°C was applied there to reduce the swelling by generating a pre-reaction thick $TiAl_3$-layer, but the decrease of swelling was very low. It was assumed that a certain amount of liquid aluminium during heating is necessary to support the sintering. According to the diffusion coefficients at 500°C of Al in Fe ($6{,}84 \cdot 10^{-16}$ cm²/s) and Fe in Al ($2{,}14 \cdot 10^{-11}$ cm²/s) the $FeAl_3$ layer is formed by the diffusion of Fe into the Al-matrix.

3.2 Swelling behaviour

In general the swelling behaviour of powder mixtures during reactive sintering is attributed to the competition of densification and homogenisation processes. In case of interacting elemental powder mixtures the homogenisation rate is much higher as the densification rate [12]. Above the melting temperature of aluminium it penetrates the iron particle and forms the intermetallic $FeAl_2$-, Fe_2Al_5 or $FeAl_3$-phase. At the spot of the aluminium matrix a pore occurs during simultaneously swelling of the iron particle. This behaviour was observed for the Ti-Al-system in detail by *Dahms et al.* [8]. *Böhm et al.* assumes that first liquid aluminium penetrates the Ti-Ti interparticle spaces and causes a macroscopic swelling of the sample. Then in stage 3 and 4 the swelling is characterised by the consumption of a high amount respectively the complete liquid aluminium by formation of $TiAl_3$ [10]. Using a model developed by *Böhm et al.* [10] the swelling can be calculated with formula (4) from the amount of aluminium:

$$\frac{\Delta l_m}{l_m} = \sqrt[3]{\frac{3 - 4 \cdot \phi_{Al} + \phi_{Al} \cdot \frac{\upsilon_{Al_3Ti} \cdot \phi_{Al}}{0{,}74 \cdot \upsilon_{Ti}}}{3 \cdot (1 - \phi_{Al})}} \tag{4}$$

where l_m = initial length of sample; Δl_m = the linear deformation; ϕ_{Al} = amount of aluminium (Ti, $FeAl_3$ $\phi_{Al} = 0{,}75$); υ = molar volumina.

The factor 0,74 is added because of the assumed porosity of the growing $TiAl_3$-layer itself equal to closely packed spherical particles. Using this formula the particle size has obviously no influence on the swelling of the sample. A remarkable agree between calculation and experiment exists up to an aluminium content of 45 at.%. Above this value the calculated swelling increasingly shows a too high value compared with the experimental value.

A second, very simple formula (5) for the calculation of macroscopic swelling of titanium aluminides during reactive sintering was proposed by *Savitskii* [11], only regarding the atomic content of Aluminium (C_S) which has passed into the titanium matrix.

$$\frac{\Delta l_m}{l_m} = \frac{C_S}{3 \cdot (1 - C_S)} \tag{5}$$

where l_m = initial length of sample; Δl = the linear deformation; C_S = at.% Al

Both formulae show an excessive increase of the swelling with increasing aluminium content which is contradictory to the sample behaviour at aluminium contents above 45 at.%. The samples show, beginning with $FeAl_2$, a degressive increase of swelling with increasing aluminium content. The swelling of $FeAl_2$ is 0,12; of Fe_2Al_5 it is 0,22 an of $FeAl_3$ it is 0,25. Reason for this could be the decreasing volume content of iron in the powder compact from 0,262 ($FeAl_2$), 0,221 (Fe_2Al_5) and 0,192 ($FeAl_3$). With decreasing volume content the distance between the iron particles gets a more and more higher value and the possible growth of the iron particles could be higher without a contact between them. Assuming that the iron particles are fully transformed in iron aluminide particles, their volumetric swelling corresponds to the ratio of the molar volumina. In the case of spherical particles their linear swelling could be easily calculated. The values are given in Tab. 1.

Tab. 1: Values for volumetric and linear swelling for spherical iron particles after transformation to iron aluminides

	molar volume iron	molar volume iron-aluminide	volumetric particle swelling $[\Delta V_p/V_{p0}]$	linear particle swelling $[\Delta l_p/l_{p0}]$
$FeAl_2$	7,13 cm³	25,06 cm³	2,51	0,53
Fe_2Al_5	2·7,13 cm³	57,98 cm³	3,07	0,59
$FeAl_3$	7,13 cm³	35,68 cm³	4,00	0,71

Macroscopic swelling of the sample should be a function of particle swelling. The unsolved problem is to know the mean interparticle distance. In principle, it is possible to suppose e.g. a primitive, a body centred or a face centred cubic arrangement for packing of iron particles into the Aluminium matrix. Corresponding calculations were done, but they didn't give satisfactory results. A second problem is the irregular particle shape of commercial reduced or atomised iron particles, so it seems more or less impossible to calculate the macroscopic linear swelling of aluminides containing low iron or titanium amounts with a relatively simple formula. In addition to that, at lower titanium or iron content a particle size depending swelling occurs [10].

3.3 Permeability

The permeability coefficients and equivalent pore diameters of aluminide filters (see Tab. 2 and Fig. 6) show interesting values compared to stainless steel and brass filters. From this point of view, the aluminide structures could replace in some applications those conventional

materials. It can be expected that the variation of particle sizes of iron and aluminium in further experiments offers the possibility to create a wider range of permeability coefficients and pore sizes.

Tab. 2: Permeability coefficients for aluminide, brass and stainless steel filter samples

Permeability coefficient	stainless steel	brass	$FeAl_2$	Fe_2Al_5	$FeAl_3$
α [m²]	$2*10^{-13}$-$1{,}8*10^{-10}$	$2*10^{-12}$-$7*10^{-10}$	$9{,}17*10^{-13}$	$4{,}22*10^{-12}$	$1{,}35*10^{-11}$
β [m]	$4*10^{-7}$- $5*10^{-7}$	$4*10^{-7}$- $5*10^{-7}$	$3{,}32*10^{-8}$	$1{,}4*10^{-5}$	$1{,}25*10^{-7}$

4 Conclusions

During reactive sintering of elemental iron and aluminium powder mixtures a swelling of the samples can be observed. This effect is usable for the creation of permeable porous structures with a potential application as filter or catalyst carrier materials. The existing formulae for the calculation of the swelling effect in elemental titanium/aluminium powder mixtures as a function of aluminium content cannot be used for the calculation of the swelling of iron aluminides with high aluminium content. One assumed reason for this behaviour is the more or less undefined particle packing combined with an irregular particle shape, which makes it very hard to calculate a reliable interparticle distance. The microstructure, permeability and porosity of the structures can be controlled by a variation of stochiometry of the intermetallic phase. The permeability coefficients and equivalent pore diameters of the aluminide structures are in the range of brass and stainless steel filters, so that they could be a possible substitute for these filter materials.

Acknowledgement

This work was performed with the gratefully acknowledged financial support of "Studiengesellschaft Stahlanwendung e.V." in the project P 317: "Entwicklung hochporöser Stahlschäume".

References

[1] Rabin, B. H. et al.: Mat. Sc. and Eng., A 153 (1992) P: 706-711
[2] Wright, J. K.: Wright, R. N.: The Minerals, Metals & Materials Society, 1994
[3] Schumann, H.: Metallographie VEB D. Verlag für Grundstoffindustrie, Leipzig 1988
[4] Wegmann, M. R.: Advances in Powder Metallurgy 1991, Vol. 2: Powder Injection Molding; English Metal Powder Industries Federation, Princeton 1991
[5] German, R.M.: Sintering Theory and Practice; John Wiley & Sons, Inc. 1996
[6] Bose, A, et al.: powder metallurgy international vol. 20 (1988) p. 25-30
[7] Wang, G.-X. et al.: Scripta Metallurgica et Materialia 26 (1992) p. 1469-1474
[8] Dahms, M. et al: Z. Metallkunde 84 (1993) Nr. 5, S. 351-357
[9] Ferreira, P. I. et al.: The Int. J. Powder Metallurgy Vol. 30 (1994), No. 3, p. 313-321
[10] Böhm, A. et al.: Z. Metallkunde 89 (1998) Nr.2; S. 90-95
[11] Savitskii, A. P.: Liquid Phase Sintering of the Systems with Interacting Components Russian Academy of Sciences, Siberian Branch; Tomsk, 1993
[12] Schatt, W.: Sintervorgänge; VDI-Verlag, Düsseldorf, 1992